Promotional Effect of La in the Three-Way Catalysis of La-Loaded Al_2O_3-Supported Pd Catalysts (Pd/La/Al_2O_3)

Yuan Jing,[†] Zhengxu Cai,[†] Chong Liu,[†] Takashi Toyao,*[†,‡] Zen Maeno,[†] Hiroyuki Asakura,[‡] Satoru Hiwasa,[⊥] Shuhei Nagaoka,*[§] Hiroshi Kondoh,[⊥] and Ken-ichi Shimizu[†,‡]

[†] Institute for Catalysis, Hokkaido University, N-21, W-10, Sapporo 001-0021, Japan

[‡] Elements Strategy Initiative for Catalysts and Batteries, Kyoto University, Katsura, Kyoto 615-8520, Japan

[⊥] Department of Chemistry, Keio University, 3-14-1 Hiyoshi, Kohoku-ku, Yokohama 223-8522, Japan

[§] Johnson Matthey Japan G.K., 5123-3, Kitsuregawa, Sakura, Tochigi 329-1412, Japan

*Corresponding authors:

Takashi Toyao and Shuhei Nagaoka

E-mail: toyao@cat.hokudai.ac.jp; Shuhei.Nagaoka@mattheyasia.com

Abstract

La-loaded Al_2O_3 (La/Al_2O_3) is a practical support for three-way catalysis (TWC) reactions. Although it has been reported that the addition of La to Al_2O_3 results in improved thermal stability to retain high specific surface areas, its effect on the catalytic reduction of NO_x ($DeNO_x$) has not been studied systematically. Herein, we describe the role of La in La/Al_2O_3-supported Pd catalysts ($Pd/La/Al_2O_3$) for TWC reactions. For that purpose, we employed various *in situ* spectroscopic studies, including IR, XAFS, and near-ambient-pressure XPS (NAP-XPS), in combination with DFT calculations. The obtained results revealed that Pd^0 species supported on La/Al_2O_3 are more electron deficient compared to those on pristine Al_2O_3 without La (Pd/Al_2O_3). Kinetic studies using powdered catalysts revealed that the addition of La suppresses the poisoning effect by CO during the $DeNO_x$ reactions. In addition to the catalytic tests with powdered catalysts, monolithic honeycomb forms of the catalysts were prepared and employed for TWC reactions, which showed that $Pd/La/Al_2O_3$ exhibits higher $DeNO_x$ activity than Pd/Al_2O_3. In this study, we also reexamined the effective loading amount of La, which has traditionally been ~3–5 wt% of La for TWC processes in order to retain the high specific surface area of the La/Al_2O_3 supports. Our investigations showed that an increased La loading (15 wt%) is even more effective for the $DeNO_x$ reactions tested in this study due to the higher reactivity toward NO and the greater suppression of the poisoning effect of CO. The developed catalyst $Pd/La(15)/Al_2O_3$ has also been tested in a commercial vehicle and been evaluated on a practical driving mode test cycle (LA-4; city cycle of US Federal and California), where it showed a better catalytic performance than the conventionally used $Pd/La(3–5)/Al_2O_3$ catalysts. Our study suggests that the loading amount of La in $Pd/La/Al_2O_3$ catalysts needs to be adjusted depending on the application systems, considering not only the support stability (surface areas) but also the promotional effect in the TWC process.

KEYWORDS: Three-way catalysis (TWC), $Pd/La/Al_2O_3$, electron deficient Pd^0, *in situ* XAFS, NAP-XPS

1. Introduction

Three-way catalysis (TWC) is regarded as the most extensively used method for controlling automotive emissions.[1–3] Much effort has been devoted to the design and development of effective catalytic materials for the TWC process, and the catalysts explored contain a variety of metals that include platinum group metals (PGMs) and other earth-abundant metals such as Fe, Ni, and Cu.[4–9] Although catalysts that contain these non-noble metal components have recently been intensively studied, practical systems still need large amounts of PGMs, such as Pd, Rh, and Pt in order to meet the very strict regulations for controlling exhaust gas emissions.[10–13] Modern commercial three-way catalysts generally consist of Pd- and Rh-based catalysts,[14,15] and therefore, the design and development of effective catalytic supports is necessary in order to maximize the activity of PGMs, especially Pd and Rh.

Among various candidates for TWC supports, La-loaded Al_2O_3 (La/Al_2O_3) is one of the most well-known and used industrial supports.[1] This is mainly due to its high specific surface area, mechanical strength, and high thermal stability.[16] Although Muraki and co-workers have reported the positive effect on the catalytic reduction of NO_x ($DeNO_x$) caused by the addition of La on Al_2O_3-based supports in the 1980s,[17–19] this research topic has not been pursued systematically in order to obtain mechanistic insight into the effect of using La/Al_2O_3 supports on the TWC processes. The authors argued that the addition of La (1) enhances the chemisorption of NO_x, which in turn leads to the selective reduction of NO_x, rather than O_2 and (2) suppresses the strong adsorption of hydrocarbons (HC) on Pd, which results in an efficient reduction of NO_x.[17–20] It should be noted here that similar promotional effects were observed upon addition of alkaline earth metals to the Pd-based catalysts.[21-23] It was also proposed by Muraki and co-workers that the high $DeNO_x$ activity of $Pd\text{-}La_2O_3/Al_2O_3$ under rich (reducing) conditions is due to the high catalytic performance of La oxides for steam-reforming and water gas shift (WGS) reactions that produce H_2, leading to a facile reduction of NO by the generated H_2.[18] Following these pioneering studies, Graham and Logan investigated the chemisorption of NO on a Pd(100) surface with over-layers of La_2O_3 and Al_2O_3.[23,24] They reported that at 300 K, NO partially dissociates on interfaces of Pd with La_2O_3 but not with Al_2O_3, suggesting that La_2O_3 enhances the dissociative adsorption of NO on the Pd surface. Sekiba and coworkers also observed that the introduction of La improves the TWC activity and attributed this higher activity to suppression of the strong adsorption of HC.[25] Skoglundh and co-workers have studied the addition of La to Pd/Al_2O_3 catalysts by a stepwise impregnation method, and observed a promotional effect of La for the conversion of NO under reducing conditions.[26] They proposed that this superior $DeNO_x$ activity of the $Pd/La/Al_2O_3$ catalysts relative to that of Pd/Al_2O_3 is caused by the formation of Pd-La oxides that promote the reduction of NO by CO. These investigations represent seminal discoveries in this research field. However, the fundamental understanding of the role of La addition in improving the catalytic performance of La/Al_2O_3-supported Pd is still insufficient compared to its industrial

importance. Comprehensive studies are necessary to further understand the behavior of Pd catalysts for TWC supported on La/Al_2O_3 supports. It should be pointed out here that most studies except the aforementioned reports have focused on the effect of La on the stability of the support, and not on the $DeNO_x$ activity. Therefore, the optimal La loading for industrial TWC processes is considered to be 3-5 wt% given that the thermal stability is maximized for this loading amount.

Recently, we have studied the role of La in $La(5)/Al_2O_3$ (La loading = 5 wt%) supports for Pd catalysts ($Pd/La(5)/Al_2O_3$) toward a NO–CO reaction,[27] which is one of the model reactions for the $DeNO_x$ chemistry.[28,29] The $Pd/La(5)/Al_2O_3$ catalyst, which contains a conventionally used amount of La, was employed for this purpose. The obtained results show that the introduction of La significantly enhances the catalytic activity toward the NO–CO reaction as a result of the efficient generation of nitrite species on the catalyst surface, and their reactivity toward CO as a reactant. It should also be informative to examine the role of La for TWC reactions under practical conditions, and it is anticipated that a more effective loading amount of La could potentially be identified for the $Pd/La/Al_2O_3$-catalyzed TWC reactions than that used for conventional industrial catalysts.

In this study, we have furthermore investigated the role of La in TWC process and the most effective loading amount of La for TWC reactions; we discovered that a loading of 15 wt%, which is higher than that for the conventional industrial catalysts (La = 3–5 wt%) optimized to retain the high specific surface area, is highly effective for the TWC process. The developed catalyst ($Pd/La(15)/Al_2O_3$) has been mounted in a commercial vehicle with a 1.5-L gasoline engine and evaluated on a LA-4 mode test cycle for practical applications. The results of various kinetic and spectroscopic studies, including *in situ* FT-IR, XAFS, and near ambient pressure X-ray photoelectron spectroscopy (NAP-XPS) in combination with density functional theory (DFT) calculations, show that Pd^0 species on the La/Al_2O_3 support are more electron deficient than Pd on Al_2O_3 in the absence of La, which leads to a higher reactivity toward NO at low temperature and a suppression of the poisoning effect of CO.

2. Experimental Section

Preparation of Materials and Catalysts

Commercially available γ-Al_2O_3 was used as the Al_2O_3 support, and the addition of La to the Al_2O_3 support was carried out as described in our previous study.[27] An aqueous solution that contains $La(NO_3)_3$ was impregnated onto the Al_2O_3 support. This was followed by drying at 120 °C for 2 h, and subsequent calcination in air at 600 °C for 2 h to yield La(x)/Al_2O_3 (x = La loading; x = 5, 15, 30 wt%). Pd/La(x)/Al_2O_3 (x = 5, 15, 30 wt%) and Pd/Al_2O_3 were prepared according to the following impregnation method: 5 g of La(x)/Al_2O_3 (or Al_2O_3) and 100 mL of an aqueous solution containing $Pd(NH_3)_2(NO_2)_2$ (obtained from Kojima Kagaku) were added to a 500 mL glass vessel. The solution was stirred for 15 min (200 rpm) at room temperature, before it was evaporated to dryness at 50 °C, dried at 90 °C (12 h), and calcined in air at 300 or 500 °C (3 h). It should be noted here that the average diameter of the Pd particles (determined by CO adsorption experiments) was adjusted to 3–4 nm by optimizing the calcination temperature. Subsequently, the catalysts were prepared by H_2 reduction of the calcined catalyst powders in a tube vessel under H_2 flow (20 mL/min) at 500 °C (0.5 h). Pd/Al_2O_3 was prepared in the same manner. Unless otherwise noted, the samples after the H_2 reduction were used for the various characterization experiments. Before each catalytic or *in situ* spectroscopic experiment, the samples were reduced again under 10% H_2/He flow (100 mL/min) at 400 °C (0.5 h).

Monolithic honeycomb catalysts were generated by coating a slurry, which was prepared from the calcined catalyst powders (1 wt% Pd), an inorganic binder, and water, onto a cordierite honeycomb (25.4 mmφ × 50 mm, 400 cells/in^2; NGK Insulators, Ltd.). This was followed by drying in air at 120 °C for 1 h and subsequent calcination at 600 °C for 2 h. The thus prepared honeycomb catalysts contained about 60 g L^{-1} of coated catalyst powder, commensurate with a total Pd loading of 0.06 g/L.

Monolithic honeycomb catalysts were aged for 4 h at 1000 °C under hydrothermal redox conditions, i.e., rich (reducing), lean (oxidizing), and stoichiometric atmospheres. The gas compositions for rich (3% CO, 3% H_2, 10% H_2O, and N_2 balance), stoichiometric (10% H_2O and N_2 balance), and lean (3% O_2, 10% H_2O, and N_2 balance) atmospheres were applied with programmed intervals of 180 s for rich, 10 s for stoichiometric, 180 s for lean, and 10 s for stoichiometric conditions. The flow rate was set to 3 L/min, which corresponds to space velocity (SV) = 7,200 h^{-1}.

Catalyst Characterization

X-ray diffraction (XRD) measurements were conducted using Cu-Kα radiation on a Rigaku Miniflex. AUTOSORB 6AG (Yuasa Ionics Co.) was used for the N_2 adsorption measurements. Bright-field scanning transmission electron microscope (BF-STEM) images and high-angle annular dark-field STEM (HAADF-STEM) images were collected using a JEM-ARM200F microscope (JEOL). CO-adsorption experiments were performed at -20 °C using BELCAT (MicrotracBEL). Temperature-

programmed reduction by H_2 (H_2-TPR) were carried out using BELCAT. For that purpose, samples were mounted in a quartz cell and heated at a temperature gradient of 10 °C min^{-1} under 5% H_2/Ar flow (20 mL min^{-1}). The gas was passed through molecular sieves (MS4Å) in order to remove water. A thermal conductivity detector (TCD) was used to detect the quantity of H_2. ^{27}Al magic angle spinning (MAS) NMR measurements were carried out on a Bruker DSX-300 spectrometer operating at 300 MHz with a 4 mm rotor. XPS measurements were performed on a JEOL JPS-9010MC (MgKα). Binding energies were calibrated with respect to C_{1s} at 285.0 eV.

***In situ* IR**

In situ IR measurements were performed at 200 °C using a JASCO FT/IR-4200 with a Mercury-Cadmium-Telluride (MCT) detector. Samples (40 mg) were pressed to make pellets (ϕ = 20 mm), which were placed in the quartz IR cell having CaF_2 windows connected to a gas flow system. The pellets were heated under a flow of 10% H_2/He (100 mL min^{-1}) at 400 °C for 0.5 h prior to the measurements. After cooling to 200 °C under the He flow, 1.0% NO/He was introduced for 600 s, before the gas was switched to He in order to allow the residual NO gas to exit. A reference spectrum, recorded at 200 °C under a flow of pure He, was subtracted from each measured spectrum.

(*In situ*) XAFS

La K-edge XAFS spectra were recorded in transmittance mode at the BL14B2 beamline (operated at 8 GeV) of SPring-8 with a Si(311) double crystal monochromator (proposal 2018A1757). Samples were sealed in polyethylene cells in air, and the spectra were measured at room temperature. The EXAFS analysis was carried out using the REX ver. 2.5 program (RIGAKU). The Fourier transformation of the k^3-weighted EXAFS was carried out over a k range of 3–12 $Å^{-1}$. The curve-fitting analysis was performed using the REX ver. 2.5 program and the parameters for each shell were provided by FEFF6.

In situ Pd K-edge XAFS spectra were measured in transmittance mode at the BL14B2 beam line of SPring-8 with a Si(311) double crystal monochromator (proposal 2018B1768). A high-sampling-rate TCD GC (490 Micro GC; Agilent Technologies Inc.) was used for the quantitative analysis of NO, CO, N_2O, and N_2. A mass spectrometer (BELMass; MicrotracBEL Corp.) was used to monitor the eluent gas. 400 mg of the samples (Pd/Al_2O_3 or $Pd/La(15)/Al_2O_3$) in pellet form (φ: 10 mm) were introduced into a quartz cell with Kapton film windows and gas lines connecting to the GC. The catalyst was pretreated under 5% H_2/He flow (200 mL min^{-1}) at 400 °C for 0.5 h, followed by cooling to 200 °C. Subsequently, 0.5% NO/He, 0.5% CO/He, and 0.5%NO+0.5%CO/He (800 mL min^{-1}) were introduced into the cell for 30 min (10 min intervals of He purge between each gas). The SV for the *in situ* Pd K-edge XAFS measurements was ~ 30, 000 h^{-1}. The EXAFS analysis was carried out as described above.

NAP-XPS

NAP-XPS experiments were conducted at the beamline 13B of the Photon Factory (PF) at the High Energy Accelerator Research Organization (KEK).[30] A powder Pd/La(15)/Al_2O_3 catalyst with a Pd loading amount of 20 wt% was used for ease of the experiments. The promotion effect of La was confirmed for this high-Pd-loading sample by carrying out NO–CO reactions (**Figure S1**). The powder catalyst, which was reduced under 10% H_2/He flow (100 mL min^{-1}) at 500 °C for 0.5 h, was once dispersed in deionized water and deposited on a Si substrate by a drop-and-dry method. The prepared substrate was then introduced into the XPS chamber. A K-type thermocouple was directly attached to the sample to measure the operating temperature. Prior to the measurement, the sample pellet was pretreated again under a CO atmosphere at 400 °C for 0.5 h. For safety reasons, CO was used as a reducing gas instead of H_2. After cooling to 50 °C, NO (100 mTorr) was introduced and the spectra were measured. All core-levels (Al 2p, C 1s, Pd 3d, N 1s) measurements were recorded continuously using a fixed photon energy (550 eV). Calibration of the binding energy was carried out using the Al 2p level (74.3 eV). The obtained XPS intensities were normalized in order to remove the effect of attenuation caused by the introduced gases. XPS spectra were analyzed using the software “fitt” by convolution of the Lorentzian and Gaussian functions with a linear background.

Catalytic Reactions

Catalytic reactions on the powdered catalysts were carried out in a flow reactor. 15 mg of the catalyst was placed in a reactor using quartz wool in the catalyst bed. After the reduction of the catalyst under 10% H_2/He flow (100 mL min^{-1}) for 0.5 h, the catalyst was cooled to 125 °C and the catalytic NO–CO reaction was started by supplying a gas mixture containing CO (0.5%) and NO (0.5%), as well as He balance at 100 mL·min^{-1} (*W*/*F* corresponds to 1.5×10^{-4} g·min·cm^{-3}). Conversions and yields of the gasses were determined by GC analysis (Shimadzu GC-8A with a SHINCARBON ST column). The yields were calculated based on the following equation.

$$NO + CO \rightarrow 0.5\ N_2 + CO_2 \qquad (1)$$

Catalytic reactions on the honeycomb form catalysts were carried out in a flow reactor using MEXA-series (Horiba Ltd.). The catalysts were placed in a tubular-type reactor, and their catalytic performance was investigated by supplying a gas mixture typically containing 0.6% CO, 420 ppm C_3H_6, 0.2% H_2, 0.1% NO, 0.6% O_2, 15% CO_2, 10% H_2O, and N_2 balance (λ = 1) at SV = 100,000 h^{-1}. Conversions of NO, C_3H_6, and CO were monitored by using an exhaust gas analyzer (ABB, AO-2020). Before each catalytic activity test, the honeycomb catalyst was pre-treated under a flow of the aforementioned gas at 400 °C for 0.5 h. The λ values were calculated using the following equation (see **Tables S1 and S2** in the Supporting Information for further details on the gas compositions).

$$\lambda = \frac{O_2 + 0.5CO + 0.5H_2O + CO_2 + 0.5NO}{0.5H_2 + CO + 1.5C_3H_6 + 0.5H_2O + CO_2} \qquad (2)$$

Practical tests using a commercial vehicle were carried out as follows. The catalysts ($Pd/La(15)/Al_2O_3$ or $Pd/La(5)/Al_2O_3$) were used in a Pd-Rh three-way catalyst with a double-layered structure. The Pd and Rh catalyst washcoats were coated on a 1.0-L ceramic monolith with a cell density of 600 in^{-2}.[31] The bottom layer consisted of Pd supported on a washcoat of the $La(x)/Al_2O_3$ (x = 5 or 15 wt%), a Ce-Zr mixed oxide, and Ba carbonate. The washcoat loading of the bottom layer was ~150 g/L with a Pd loading of 3 g/L. The top layer consisted of Rh supported on a washcoat of another Ce-Zr mixed oxide and $La(5)/Al_2O_3$. The washcoat loading of the top layer was ~60 g/L with a Rh loading of 0.3 g/L. The thus prepared three-way catalysts were bench-aged using a 1.8-L gasoline engine with a peak temperature of 950 °C for 75 hours. The aged catalysts were mounted in a commercial vehicle with a 1.5-L engine, and the vehicle emission test of LA-4 driving cycle (city cycle of US Federal and California) were conducted. The concentrations of NO_x ($NO + NO_2$), CO, and the total hydrocarbons (THC), as well as the catalyst-bed temperature and air-to-fuel ratio (AFR) were monitored by employing a Horiba MEXA series.

DFT calculations

All spin-polarized calculations were conducted using Vienna *Ab Initio* Simulation Package (VASP),[32,33] using projector-augmented wave potentials[34] and the Perdew-Burke-Ernzerhof (PBE) functional.[35] The DFT-D3 method with Becke-Johnson damping dispersion correction was employed to take into account the dispersion interaction.[36,37] The original γ-Al_2O_3(100) surface structure was modelled according to a previous study by Raybaud and co-workers (**Figure S2**).[38] The structural model contains a (2 x 2) supercell, a four-layer-thick slab, and 10 Å of vacuum with 160 atoms (lattice parameters for the surface: a = 10.97 Å, b = 16.54 Å). The slab model was calculated with 2 × 1 × 1 k-points mesh and an energy cutoff of 400 eV. The (100) surface was employed in this study because it is the most stable surface for γ-Al_2O_3. The first two layers of γ-Al_2O_3 relative to the surface were allowed to relax for the geometry optimization, while the two bottom layers were fixed. The criterion of the convergence was set to F_{max} < 0.03 eV/Å, where F_{max} is the maximum force that acts on the mobile atoms. For Pd_{13} clusters, the new biplanar (NBP) model was employed.[38] The adsorption energy of Pd_{13} on the alumina support (E_{ads}) can be calculated according to:

$$E_{ads} = E(Pd_{13}/Support) - E(Pd_{13}) - E(Support) \quad (3)$$

where $E(Pd_{13}/Support)$, $E(Pd_{13})$, and $E(Support)$ refer to the electronic energy of the supported system, the Pd_{13} cluster, and the support slab without the Pd_{13} cluster, respectively. In addition, interaction energies of the Pd_{13} clusters and the alumina support are defined by:

$$E_{int} = E(Pd_{13}/Support) - E(Pd_{13}') - E(Support') \quad (4)$$

where $E(Pd_{13}')$ is the energy of the Pd_{13} cluster having the deformed geometry after its adsorption on

the support surface, and E(Support') is the energy of the surface fragment having the deformed geometry after adsorption of the Pd_{13} cluster. Deformation energies are defined by the following Eqs. (5) and (6) for the support and the Pd_{13} cluster, respectively. They enable quantifying the influence of the shape adaptation on the adsorption event. Eqs. (7) and (8) describe the total deformation energy, which links the adsorption, interaction, and deformation energies.

$$E_{def\_Support} = E(\text{Support'}) - E(\text{Support}) \quad (5)$$

$$E_{def\_Pd13} = E(Pd_{13}') - E(Pd_{13}) \quad (6)$$

$$E_{def\_total} = E_{def\_Support} + E_{def\_Pd13} \quad (7)$$

$$E_{ads} = E_{int} + E_{def\_total} \quad (8)$$

Bader charge analyses were carried out on the same system.

3. Results and Discussion

Catalysts Characterization

The preparation conditions and the average Pd particle diameters for the Pd/Al_2O_3 catalyst and a series of $Pd/La(x)/Al_2O_3$ (x = 5, 15, 30 wt%) catalysts used in this study are summarized in **Table 1**. It should be noted here that some information and data for Pd/Al_2O_3 and $Pd/La(5)/Al_2O_3$ were taken from our previous report.[27] Catalysts containing Pd particles with an average diameter of 3–4 nm were prepared by optimizing the calcination temperature prior to the H_2 reduction process. Powder XRD patterns of the $Pd/La(x)/Al_2O_3$ catalysts show peaks assignable to γ-Al_2O_3 (**Figure S3A**).[27] This result indicates that all the Al_2O_3 and $La(x)/Al_2O_3$ supports used in this study are mainly comprised of the γ-Al_2O_3 phase.[27] However, the peak intensities decreased for samples containing higher proportions of La, indicating that these are of lower crystallinity compared to pristine γ-Al_2O_3. Peaks assignable to La_2O_3, $LaAlO_3$, or Pd species were not observed.[27] The ^{27}Al MAS NMR spectra (**Figure S3B**) of all catalysts exhibit two features at approximately 13 and 73 ppm, which were attributed to Al^{3+} cations in octahedral and tetrahedral coordination environments, respectively.[39–41] Pentacoordinated Al species that are typically observed at 35-40 ppm were not observed in our experiments. Reference compound $LaAlO_3$ exhibited only one peak at 12 ppm, indicating that it contains exclusively Al species that are octahedrally coordinated by oxygen. These ^{27}Al MAS NMR results are consistent with the XRD results, and thus corroborate that our catalysts are comprised predominantly of the γ-Al_2O_3 phase. N_2 adsorption isotherms are given in **Figure S3C**. The BET specific surface areas (S_{BET}) of the Pd/Al_2O_3 and $Pd/La(x)/Al_2O_3$ catalysts are summarized in **Table 1**. The S_{BET} gradually decreased with increasing La loading. XPS analyses were carried out for $La(15)/Al_2O_3$ and $LaAlO_3$, as shown in **Figure S3D**. The XPS spectra exhibit signals that correspond to $3d_{5/2}$ and $3d_{3/2}$ core levels and their satellite peaks.[27,42] $La(15)/Al_2O_3$ shows the main $3d_{5/2}$ peak at ~834.3 eV, which is higher than those seen in the spectrum for $LaAlO_3$ (~833.4 eV) and La_2O_3 (~833.9 eV),[27] suggesting that the La species in $La(15)/Al_2O_3$ are well dispersed.[27,42,43] H_2-TPR profiles of Pd/Al_2O_3, $La(15)/Al_2O_3$, and $Pd/La(15)/Al_2O_3$, which were measured under a 5% H_2/Ar flow (30 mL/min), are shown in **Figure S4**. The peak assignable to the reduction of PdO_x species at ca. 150 ˚C shifted to higher temperatures upon introduction of La in the support. This observation indicates that the introduction of La prevents the reduction of PdO_x species.

Table 1. Preparation conditions and textual properties of Pd/Al_2O_3 and $Pd/La(x)/Al_2O_3$.

Catalyst	$T_{calcination}$ / ˚C	$T_{H2\ reduction}$ / ˚C	S_{BET}[a] / $m^2\ g^{-1}$	Pd particle diameter[b] / nm
Pd/Al_2O_3[c]	500	500	156	3.4
$Pd/La(5)/Al_2O_3$[c]	500	500	148	3.1
$Pd/La(15)/Al_2O_3$	500	500	129	3.7
$Pd/La(30)/Al_2O_3$	300	500	74	3.8

[a] Determined by N_2 adsorption. [b] Estimated by CO adsorption at -20 ˚C. [c] The information and data for Pd/Al_2O_3 and $Pd/La(5)/Al_2O_3$ were taken from our previous report.[27]

La(15)/Al_2O_3 and Pd/La(15)/Al_2O_3 were subjected to HAADF-STEM measurements. La in La(15)/Al_2O_3 is atomically dispersed, as shown in **Figures 1** and **S5**. This result is consistent with earlier findings for a similar La/Al_2O_3 system.[27,44–47] Moreover, the obtained images show that Pd nanoparticles in Pd/La(15)/Al_2O_3 exhibit an average particle size of 3–4 nm. The results of the La K-edge XAFS analysis for the Pd/La(x)/Al_2O_3 samples (x = 15 and 30 wt%) and their reference compound ($LaAlO_3$) are shown in **Figure S6**. $LaAlO_3$ is a perovskite material with a cubic structure. The first coordination environment around La consists of 12 O atoms with the same distance.[44] The EXAFS Fourier transform for $LaAlO_3$ shows La–Al and La–La at approximately 2.9 and 3.5 Å, respectively. For the Pd/La(x)/Al_2O_3 (x = 15, 30 wt%) samples, two peaks were observed at ca. 1.2 and 2.0 Å. It has been reported that the peak at 2.0 Å is due to La–O bonds, while the smaller peak arises from a side lobe of the La–O bonds due to the nonlinearity of their phase shifts.[44] The same feature was observed for Pd/La(5)/Al_2O_3 (data not shown).[27] A curve-fitting analysis of the EXAFS spectra is summarized in **Table S3**, which shows that the spectra of all Pd/La(x)/Al_2O_3 samples comprise only one La–O contribution. These results suggest that La is highly dispersed, which is in accordance with the aforementioned results of the XRD, XPS, and STEM measurements.

Pd K-edge XAFS measurements for Pd/Al_2O_3 and Pd/La(15)/Al_2O_3 (**Figure 2 and Table 2**) were carried out under a flow of 5% H_2/He at 200 °C after H_2 reduction at 400 °C. EXAFS Fourier transforms of Pd/Al_2O_3 and Pd/La(15)/Al_2O_3 showed only one distinct peak, which corresponds to the Pd–Pd bonds, indicating that the Pd species in Pd/Al_2O_3 and Pd/La(15)/Al_2O_3 are in metallic states. On the other hand, the XANES spectra showed that the edge position for Pd/La(15)/Al_2O_3 is slightly positively shifted compared to that of Pd/Al_2O_3, even though their Pd particle sizes are almost identical.

To further study the electronic properties of Pd on the La-modified Al_2O_3 surfaces, DFT calculations were employed. We modelled La_5-Al_2O_3 by substituting five superficial Al atoms with La atoms. For the choice of the substituted Al atoms, we examined all possible permutations of substitution and confirmed that the chosen model is the most stable. The optimized structures for Pd_{13}/Al_2O_3, La_5-Al_2O_3, and Pd_{13}/La_5-Al_2O_3 are shown in **Figure S7**. For Pd_{13}/Al_2O_3, E_{def_Pd13}, E_{ads}, and E_{int} values of 1.45, -5.60, and -7.05 eV, respectively, were determined. For Pd_{13}/La_5-Al_2O_3 on the other hand, we determined values of 1.24, -6.05, and -7.29 eV. These results show that the addition of La could potentially lead to a stabilization of Pd on the support. Moreover, we calculated the average Bader charge of Pd_{13} for Pd_{13}/Al_2O_3 (-0.036) and Pd_{13}/La_5-Al_2O_3 (-0.015), which indicates that Pd^0 species on La/Al_2O_3 is more electron deficient than Pd on pristine Al_2O_3. This result is in consistent with the aforementioned results of the Pd K-edge XAFS measurements.

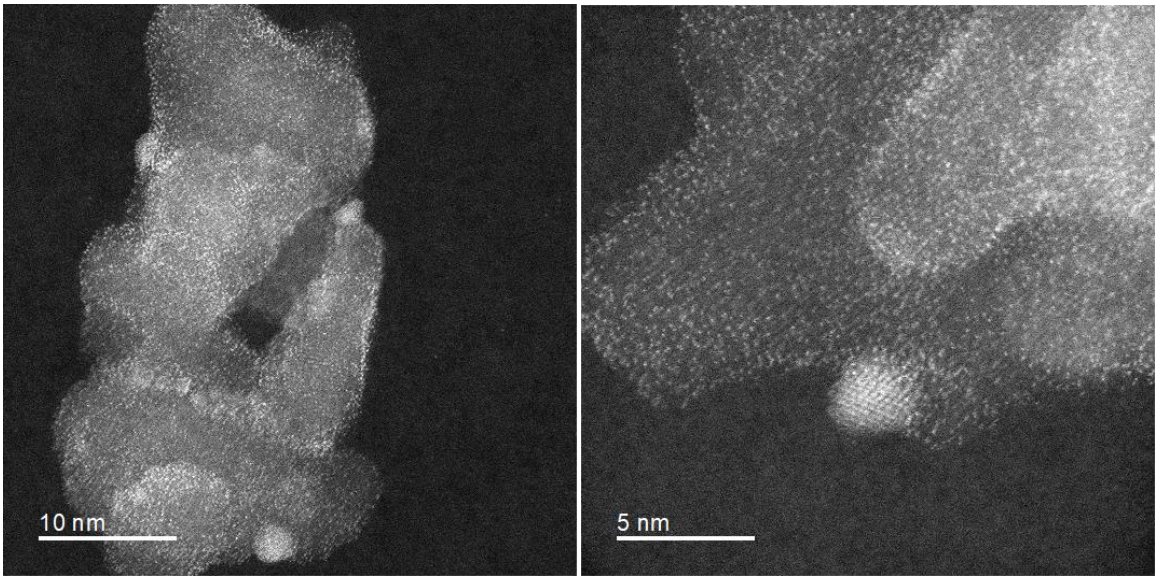

Figure 1. HAADF-STEM images of Pd/La(15)/Al_2O_3.

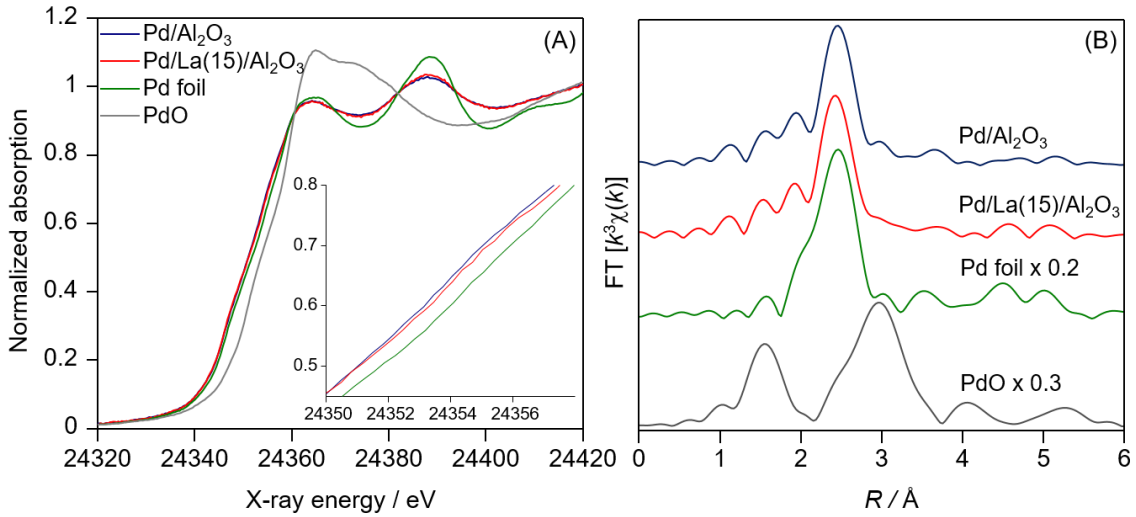

Figure 2. *In situ* Pd K-edge (A) XANES spectra and (B) k^3-weighted EXAFS Fourier transforms of Pd/Al_2O_3, $Pd/La(15)/Al_2O_3$, Pd foil, and PdO. The spectra of Pd/Al_2O_3 and $Pd/La(15)/Al_2O_3$ were collected under a flow of 5% H_2/He (200 mL/min) at 200 °C after H_2 reduction at 400 °C. The spectra of Pd foil and PdO were collected at room temperature in air.

Table 2. Curve-fitting analysis of the Pd K-edge EXAFS of Pd/Al_2O_3 and $Pd/La(15)/Al_2O_3$.

Sample	Shell	CN [a]	*R* (Å) [b]	σ (Å) [c]	R_f (%) [d]
Pd/Al_2O_3	Pd–Pd	3.1	2.67	0.11	1.1
$Pd/La(15)/Al_2O_3$	Pd–Pd	3.3	2.67	0.10	1.1

[a] Coordination number. [b] Bond distance. [c] Debye-Waller factor. [d] Residual factor.

Promotional effect of La on the NO reduction activity

NO–CO reactions with a powdered sample of Pd/La(15)/Al_2O_3 were performed as shown in **Figure 3A**. It should be noted here that the relative quantities refer to the reactants (NO and CO) and were obtained from eqn. (1). Pd/La(15)/Al_2O_3 shows a higher catalytic activity than Pd/Al_2O_3 and a comparable activity to Pd/La(5)/Al_2O_3 (NO conversion at 150 °C = 33.6% for Pd/La(15)/Al_2O_3 and 36.2% for Pd/La(5)/Al_2O_3).[27] This result confirms that La addition onto Al_2O_3 affects not only the stability, but also the catalytic activity in the NO–CO reaction.[27] In order to further investigate the role of La in the NO–CO reaction, reaction orders with respect to NO and CO were determined for Pd/La(15)/Al_2O_3 and Pd/Al_2O_3 from the steady-state reaction rate in a stream of NO and CO with different partial pressures (**Figure 3B**). It should be noted that the reaction rates were determined at an NO conversion < 30%. Reactions involving CO are often of negative order with respect to CO.[46,48] The strong binding of CO to the metal surface is usually commensurate to catalyst inhibition, i.e., CO acts as a catalyst poison that needs to desorb prior to the reaction, which in turn leads to negative-order kinetics for such reactions on PGMs. This phenomenon was also observed for Pd/Al_2O_3, where the reaction order with respect to CO is -0.28, indicating that CO acts as a poison for Pd. Conversely, for Pd/La(15)/Al_2O_3, the reaction order with respect to CO is positive (+0.35), which indicates that CO is not a catalyst poison for Pd/La(15)/Al_2O_3. Similar behavior was observed by Datye and co-workers for the oxidation of CO with O_2 over a Pd (2.5 wt%) catalyst supported by La/Al_2O_3 (4 wt% La_2O_3; W. R. Grace (MI-386)).[46] They attributed this to single atom nature of the Pd species. In addition, it is well known that the π back-donation from the transition metal surface to the adsorbate CO strongly contributes to the adsorption strength.[49,50] This contribution is weakened when Pd is positively charged, thus leading to a weaker adsorption of CO. Consequently, CO does not act as a catalyst poison for Pd/La(15)/Al_2O_3. We have also examined the adsorption energy of CO by using DFT calculations (Figure S8). The adsorption energy of CO on Pd_{13}/La_5-Al_2O_3 (E_{ads} = -2.18 eV for a hollow site and -1.62 eV for an ontop site) are smaller than those on Pd_{13}/Al_2O_3 (E_{ads} = -2.40 eV for a hollow site and -2.24 eV for an ontop site). It should also be noted here that the most stable structures were employed for this investigation for each model and adsorption site. This result also suggests that the addition of La leads to a weaker adsorption of CO. The reaction orders with respect to NO over Pd/La(15)/Al_2O_3 (+0.43) and Pd/Al_2O_3 (+0.83) showed a value for Pd/La(15)/Al_2O_3 that is in accordance with the results obtained by the *in situ* IR spectroscopy reported in our previous study,[27] which suggests that the promotional effect of La arises from the efficient generation of nitrite species on the catalyst surface and from their reactivity toward CO.

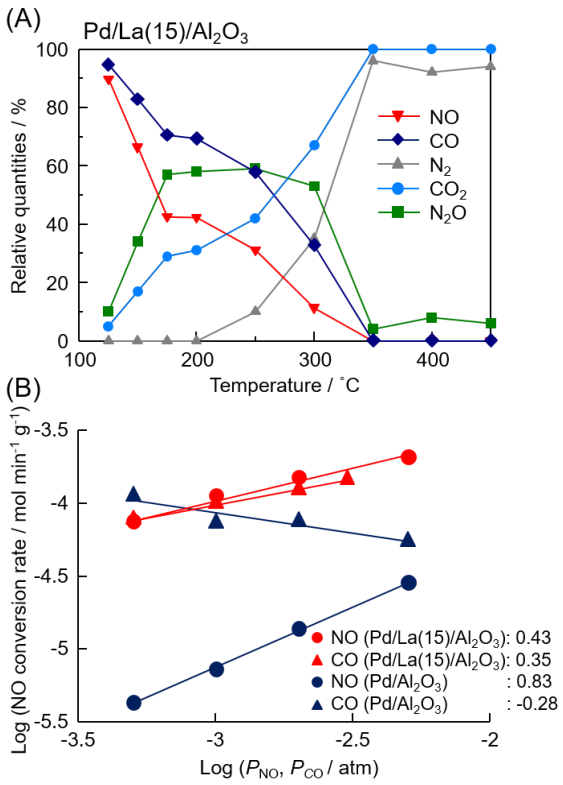

Figure 3. (A) Catalytic NO–CO reaction over a powdered sample of $Pd/La(15)/Al_2O_3$. Conditions: 0.5% CO, 0.5% NO, He balance; Catalyst weight = 15 mg. (B) Partial pressure dependence of the conversion rate of NO and the reaction order in the NO–CO reaction over powdered samples of $Pd/La(15)/Al_2O_3$ and Pd/Al_2O_3 at 150 ˚C. Conditions: 0.05–0.5% CO, 0.05–0.5% NO, He balance.

In order to get further insights into the effect of La on the reactivity of Pd/Al_2O_3 and $Pd/La(15)/Al_2O_3$ toward NO, *in situ* Pd-K edge XAFS measurements were carried out under a flow of NO, CO, NO+CO at 200 °C after H_2 reduction at 400 °C.[51] For that purpose, 0.5% NO/He, 0.5% CO/He, and 0.5%NO+0.5%CO/He (800 mL min^{-1}) were introduced consecutively into the cell (30 min for each gas). The SV for the *in situ* Pd K-edge XAFS measurements was ~ 30,000 h^{-1}. **Figure 4** shows the corresponding XANES and the FT of the k^3-weighted EXAFS (without correction of the phase shift) of Pd/Al_2O_3 and $Pd/La(15)/Al_2O_3$ measured under a flow of 0.5% NO/He. The XANES of $Pd/La(15)/Al_2O_3$ show that the absorption edge shifts to higher energy upon introduction of NO. The FT of the k^3-weighted EXAFS spectra show that a peak corresponding to Pd–Pd (ca. 2.5 Å) decreased while a peak corresponding to Pd–O (ca. 1.6 Å) increased, indicating that Pd is oxidized by NO. During that event, N_2O was formed over the $Pd/La(15)/Al_2O_3$ catalyst as detected by the high-sampling-rate thermal conductivity detector GC (**Figure 5A**). The Pd^0 fraction ($Pd^0/(Pd^0+Pd^{II})$), derived from the linear combination fitting on the XANES analysis, also showed the original Pd species was oxidized by the introduced NO (**Figure 5B**). The Pd^0 fraction 30 min after the introduction of NO was determined to be 0.58. Subsequently, the partly oxidized Pd species were reduced by the introduction of CO and the Pd species adopted an almost metallic state (Pd^0 fraction = 0.86) 30 min after the introduction of CO. It should be noted here that the formation of CO_2 was detected upon introduction

of CO. Moreover, the Pd species remained almost unchanged under a flow of 0.5%NO+0.5%CO/He gas, and N_2O, N_2, and CO_2 were detected as the gas-phase products. The coordination numbers for the Pd–Pd shells ($CN_{Pd–Pd}$) were obtained from a curve-fitting analysis of the EXAFS (**Figure 5C**). The $CN_{Pd–Pd}$ values decreased under a flow of NO, while a subsequent introduction of CO led to an increase of the $CN_{Pd–Pd}$, which is consistent with the results of the XANES analysis. These results indicate that the Pd species undergo a redox cycle in the presence of NO as an oxidizing gas and in the presence of CO as a reducing gas during the NO–CO reaction. A comparison with Pd/Al_2O_3 revealed the same redox behavior of the Pd species upon introduction of the reactant gasses. The changes to the Pd^0 fraction upon introduction of NO was smaller than that observed in $Pd/La(15)/Al_2O_3$, suggesting that the presence of La induces efficient oxidation of Pd by NO. On the other hand, the $CN_{Pd–Pd}$ value for Pd/Al_2O_3 was smaller than that for $Pd/La(15)/Al_2O_3$. We also discovered that the Pd–O contribution did not appear in the FT of the k^3-weighted EXAFS spectra of Pd/Al_2O_3. These results suggest that metallic Pd species were oxidized for Pd/Al_2O_3 upon introduction of NO, albeit that PdO species were not formed, which stands in contrast to the case of $Pd/La(15)/Al_2O_3$. This could potentially be interpreted in terms of the highly dispersed nature of the Pd species on the Al_2O_3 support without La after the NO treatment for 30 min. In order to establish conditions identical to those in the XAFS analysis, we exposed Pd/Al_2O_3 to a flow of 0.5% NO/He at 200 ˚C, and subsequently recorded HAADF-STEM images (**Figure 6**). Although only Pd nanoparticles were observed for the fresh Pd/Al_2O_3 sample, highly dispersed Pd species including individual Pd atoms were observed for the sample after the NO treatment. As such highly dispersed Pd species should not form PdO species with definite Pd–O bonds, the Pd–O contribution did not appear for Pd/Al_2O_3. This interpretation would imply that La stabilizes the supported Pd particles. It is worth mentioning here that Cargnello and co-workers have recently reported similar phenomena for Pd/Al_2O_3 catalysts during the catalytic oxidation of methane.[52] The authors have reported that the supported Pd nanoparticles lose activity for the oxidation of methane by decomposition into inactive single atoms.

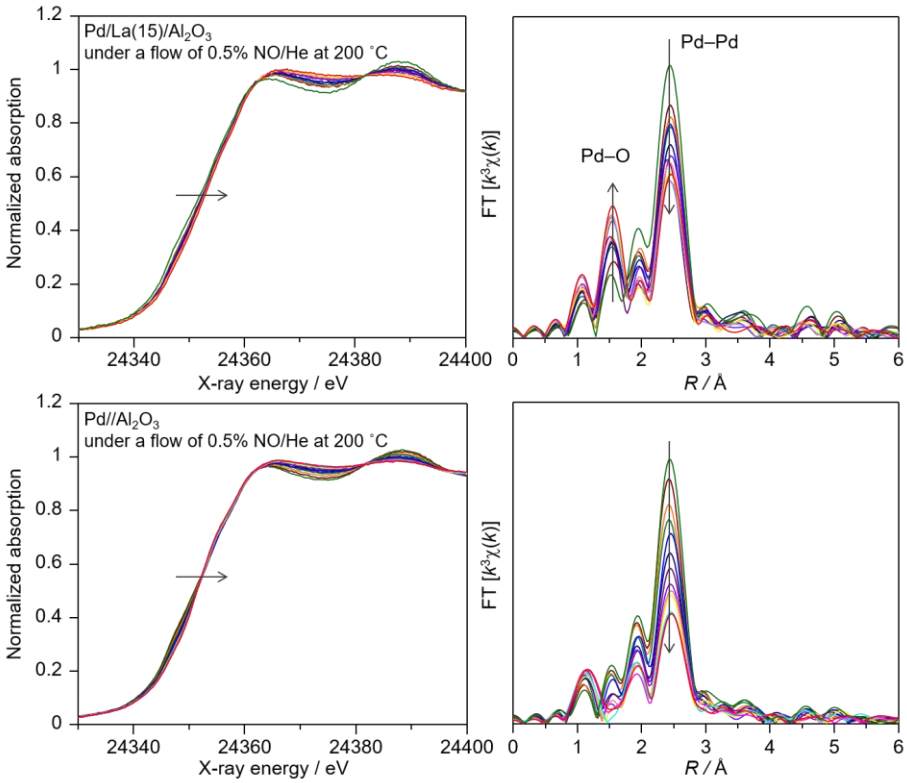

Figure 4. *In situ* Pd K-edge XANES spectra and k^3-weighted EXAFS Fourier transforms of $Pd/La(15)/Al_2O_3$, performed under a flow of 0.5% NO/He (800 mL/min) at 200 °C after H_2 reduction at 400 °C.

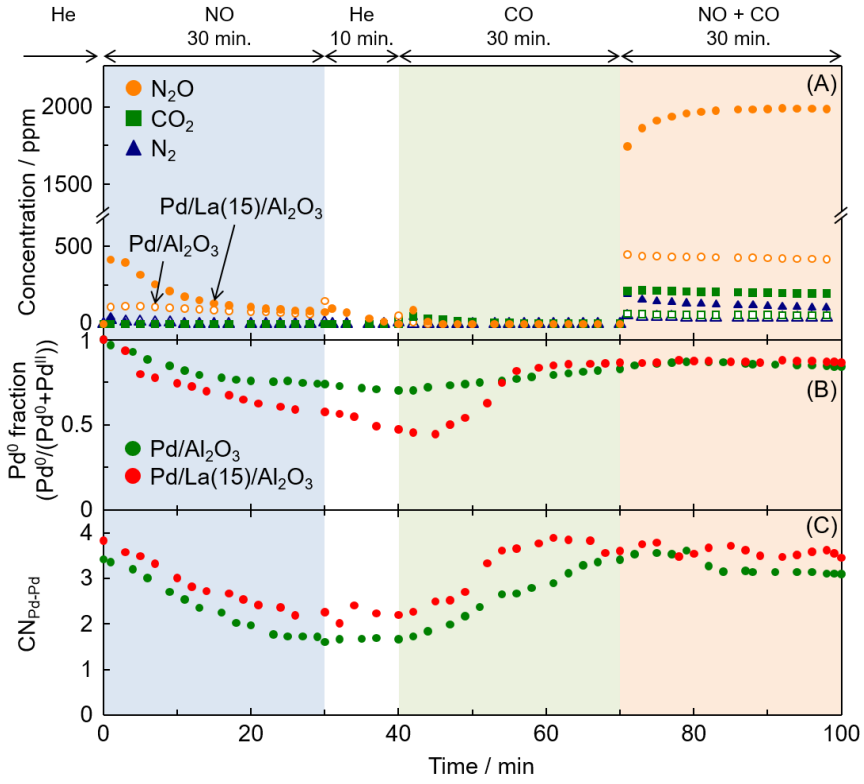

Figure 5. Results of the *in situ* Pd K-edge XAFS measurements. Changes in (A) the product concentrations in the gas phase, (B) fraction of Pd^0, and (C) CN_{Pd-Pd} under a flow of NO, CO, and NO+CO at 200 °C.

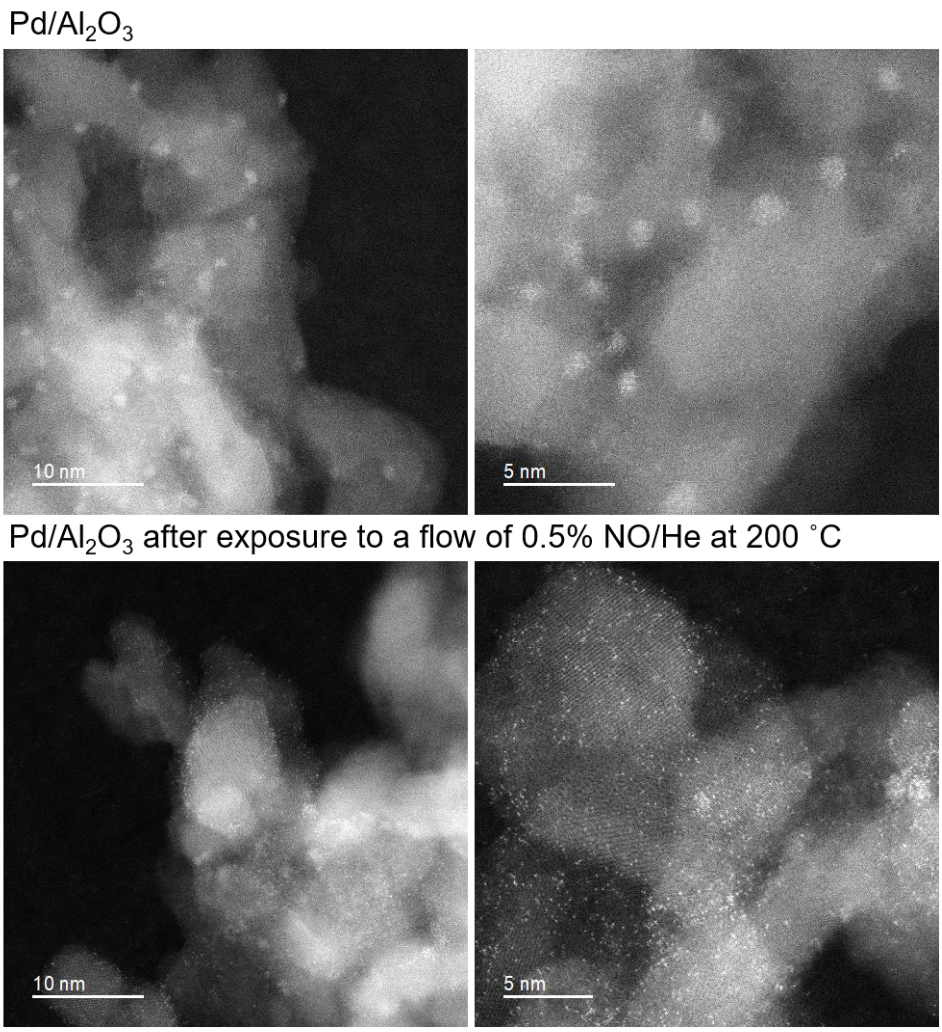

Figure 6. HAADF-STEM images of Pd/Al_2O_3 before and after exposure to a flow of 0.5% NO/He at 200 ˚C.

Subsequently, temperature-programmed surface reactions (TPSRs) were conducted in order to gain further insight into the reactivity of $Pd/La(15)/Al_2O_3$ and Pd/Al_2O_3 toward NO (**Figure 7**). After the pretreatment with H_2, the catalyst was exposed to 0.5 % NO/He flow for 10 min at 40 °C. After purging under He for 30 min, the catalyst was then heated to 500 °C in a flow of He (10 °C min^{-1}), and the gas-phase products were monitored by mass spectrometry. Although no obvious signals due to products such as N_2O and N_2 were observed below 100 °C over Pd/Al_2O_3, $Pd/La(15)/Al_2O_3$ produced N_2O even below 100 °C, which corroborates the notion that the presence of La induces higher reactivity of Pd toward NO at lower temperature. **Figure 8** shows the *in situ* IR spectra of species adsorbed on $Pd/La(15)/Al_2O_3$, Pd/Al_2O_3, and $La(15)/Al_2O_3$ after the introduction of NO at 50 °C. Various kinds of adsorbed NO_x species appear in the 1100-1800 cm^{-1} region after the introduction of NO.[27] Specifically, peaks that were attributed to nitrite arise at ca. 1192 and 1230 cm^{-1}.[27,53] The intensities of these absorption peaks over $Pd/La(15)/Al_2O_3$ are much higher than those observed over Pd/Al_2O_3, indicating that higher amounts of surface nitrite species are generated over $Pd/La(15)/Al_2O_3$. Also, these peaks were virtually negligible over $La(15)/Al_2O_3$, i.e., in the absence of Pd nanoparticles,

indicating the importance of the combination of Pd nanoparticles and La(15)/Al_2O_3 as a support. The absorption bands at ca. 1293 cm^{-1} can be assigned to both nitrates and nitrites.[27,53] The bands in the 1300-1650 cm^{-1} region appeared due to the presence of a variety of nitrate species with different adsorption modes.[27,54,55] The bands in the 1600-1800 cm^{-1} region were assigned to free nitrate ions[27,53] and/or to Pd-adsorbed NO.[27,53,56] The combined results of the NO-TPSR and the *in situ* IR spectroscopy suggest that the disproportionation reaction of NO over Pd/La(15)/Al_2O_3 affords nitrous oxide and nitrite even at low temperatures (< 100 ˚C).

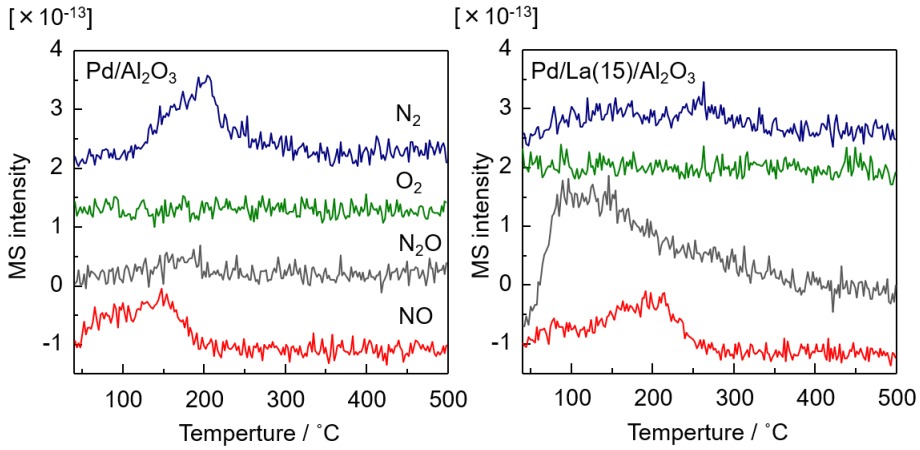

Figure 7. NO TPSR experiments for Pd/La(15)/Al_2O_3 and Pd/Al_2O_3. After the pretreatment with H_2, a catalyst was exposed to 0.5 % NO/He flow for 10 min at 40 °C. After purging in He for 30 min, the catalyst was heated to 500 °C in a flow of He (10 °C min^{-1}).

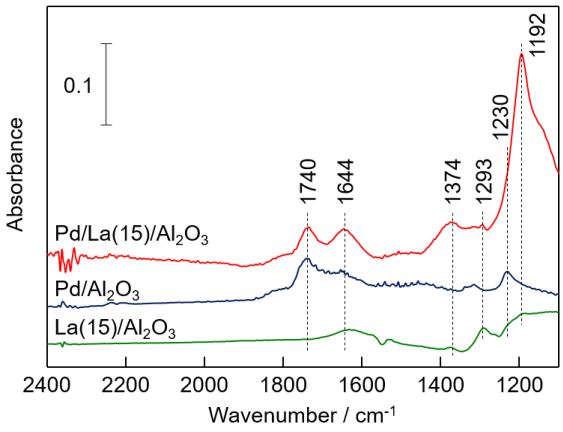

Figure 8. *In situ* IR spectra of species adsorbed on Pd/La(15)/Al_2O_3, Pd/Al_2O_3, and La(15)/Al_2O_3 at 50 ˚C. Spectra were recorded under He flow after the NO feed.

In order to obtain further insights into the NO-activation process over Pd/La(15)/Al_2O_3, NAP-XPS measurements were carried out. For this purpose, a powdered sample of a high-Pd-loaded Pd/La(15)/Al_2O_3 catalyst (Pd loading: 20 wt%), for which the promotional effect of La was confirmed by NO–CO reactions (**Figure S1**), was used for ease of the experiments. It should be noted here that the average Pd particle size for this Pd/La(15)/Al_2O_3 catalyst was determined to be 12.2 nm by a CO-

adsorption measurement at -20 ˚C. After the pretreatment, the sample was cooled to 50 °C, and subsequently, NO (100 mTorr) was introduced. **Figure 9** shows an XPS spectrum of the N 1s region for Pd/La(15)/Al_2O_3, measured under an NO atmosphere (100 mTorr). The spectrum of the NO-adsorbed Pd/La(15)/Al_2O_3 contains four peaks at ca. 404, 401, 398, and 393 eV, which can be assigned to the surface-adsorbed nitrite (NO_2^-), molecularly adsorbed NO species (NO_{ad}), atomic nitrogen (N_{ad}), and NO species bound on the Si substrate, respectively.[57,58] The presence of the peak associated with N_{ad} indicates that NO is dissociated over Pd/La(15)/Al_2O_3 even at 50 °C. We also confirmed that the nitrite species is formed in accordance with the results of *in situ* IR study.

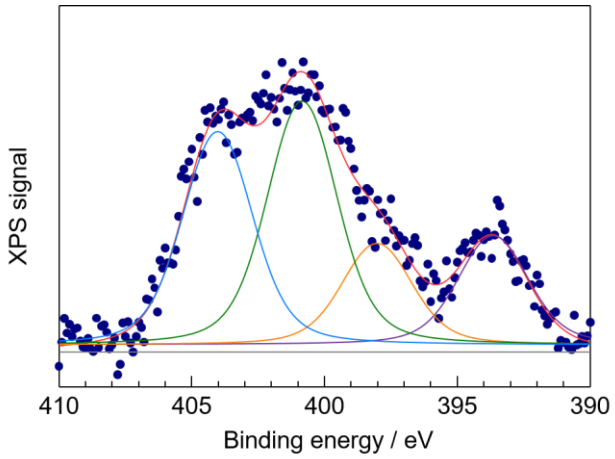

Figure 9. N 1s XPS spectrum of Pd/La(15)/Al_2O_3 (Pd loading: 20 wt%), measured upon exposure to NO (100 mTorr) at 50 ˚C. Navy dots: raw spectrum; red line: sum; blue line: surface-adsorbed nitrite (NO_2^-); green line: molecularly adsorbed NO (NO_{ad}); yellow line: atomic nitrogen (N_{ad}); purple line: NO species bound on the Si substrate; grey line: background.

Three-way catalytic reactions using monolithic honeycomb catalysts

Results of TWC light-off tests over monolithic honeycomb forms of Pd/La(x)/Al_2O_3 (x = 0, 5, 15, 30 wt%) catalysts are shown in **Figure 10**. The catalytic performances were evaluated in light-off mode under 1-Hz perturbated gasses between λ = 0.95 and λ = 1.05 at SV = 100,000 h^{-1}. Gas mixtures used for this test contained 0.6-2.4% CO, 420 ppm C_3H_6, 0.2% H_2, 0.1% NO, 0.6-1.65% O_2, 15% CO_2, 10% H_2O, and N_2 balance. It should be noted here that the honeycomb catalyst was pre-treated under a flow of the aforementioned gas at 400 °C for 0.5 h prior to each catalytic activity test. The conversion of NO, CO, and C_3H_6, which was continuously monitored, showed that the efficiency of Pd/La(15)/Al_2O_3 to remove these gasses was higher than that of Pd/Al_2O_3, indicating that La efficiently promotes the TWC reaction. In addition, the activity of Pd/La(15)/Al_2O_3 was comparable or slightly higher for the conversion of NO than that of the conventional Pd/La(5)/Al_2O_3 catalyst. We also observed that Pd/La(30)/Al_2O_3 exhibited lower activity for the TWC process, which demonstrates that an overloading with La is ineffective. Furthermore, the durability of these catalysts was studied using aged catalysts (for procedural details, see the Experimental Section). This is a highly important investigation, as in practice, catalysts are exposed to very harsh conditions, which they should ideally withstand for a long time. Although their activity decreased by the aging treatment, the aged Pd/La(15)/Al_2O_3 monolithic honeycomb catalyst still exhibited better performance than the other catalysts. This result suggests that Pd/La(15)/Al_2O_3, whose La loading is higher than that for the conventionally used industrial catalysts (La = 3–5wt%) optimized to keep high specific surface area, could potentially serve as a highly effective promoter for TWC processes even after hydrothermal aging.

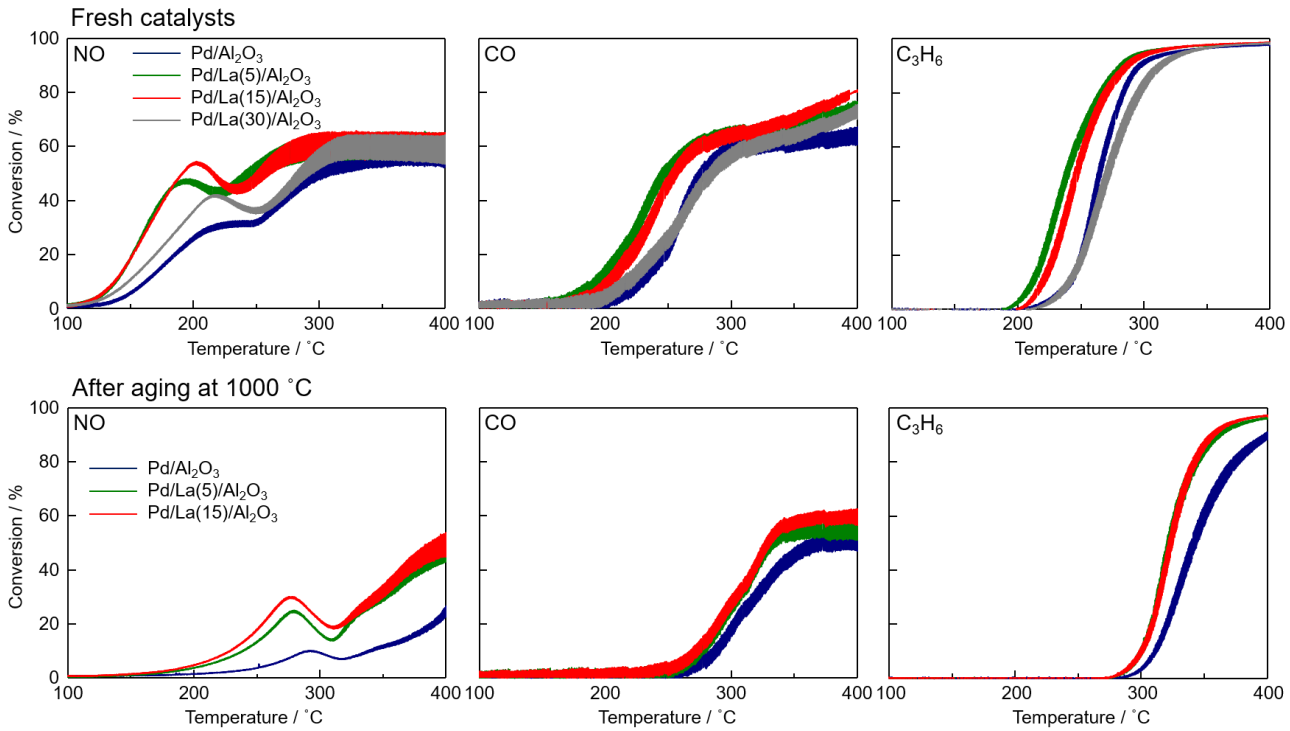

Figure 10. NO, CO, and C_3H_6 conversions for TWC light-off tests over the fresh and aged $Pd/La(x)/Al_2O_3$-coated honeycomb catalysts (x = 0, 5, 15, 30 wt%) under 1-Hz perturbated gasses between λ = 0.95 and λ = 1.05. Heating rate: 25 ˚C/min; Gas: CO (2.4-0.6%), C_3H_6 (420 ppm), H_2 (0.8%), NO (0.1%), O_2 (0.6-1.65%), CO_2 (15%), H_2O (10%), N_2 balance; SV = 100,000 h^{-1}.

The catalysts, after aging at 1000 °C for 4 h, were also characterized by XRD and N_2 adsorption techniques (**Figure 11**). It should be noted that the powdered catalysts were subjected to the aging treatment and analyzed for this purpose. Powder XRD patterns of the $Pd/La(x)/Al_2O_3$ (x = 0, 5, 15, 30 wt%) catalysts after aging at 1000 °C for 4 h (**Figure 11A**) show peaks assignable to $LaAlO_3$ in the diffraction patterns of $Pd/La(15)/Al_2O_3$ and $Pd/La(30)/Al_2O_3$, whereas these peaks were virtually negligible for the conventionally used catalyst $Pd/La(5)/Al_2O_3$. Peaks due to La_2O_3, Pd_3La alloy, or La_4PdO_7 were not seen in any of the XRD patterns.[59,60] S_{BET} values for the aged catalysts were determined from N_2-adsorption isotherms and are summarized in **Figure 11B** together with those of the fresh samples. $Pd/La(5)/Al_2O_3$ retained the highest S_{BET} value after hydrothermal aging; this is consistent with previous studies on the La/Al_2O_3 system, which focused on retaining high surface areas for their designated purpose as TWC supports.

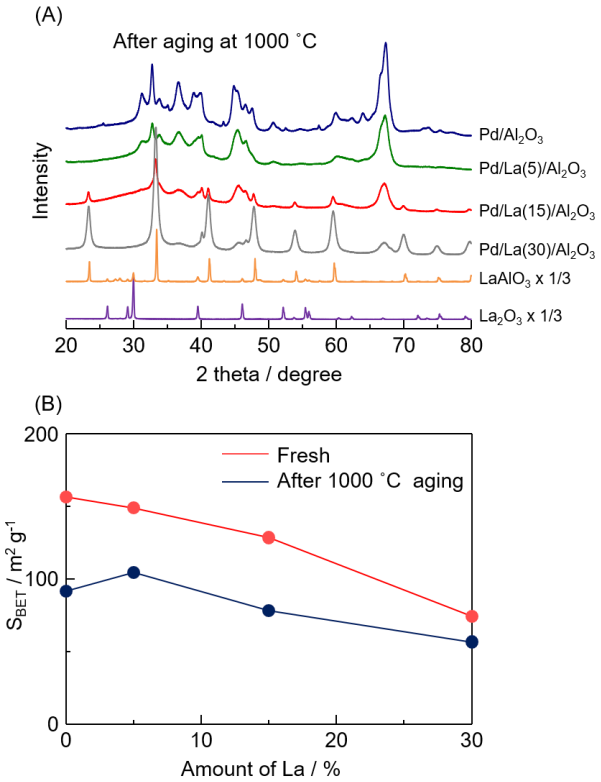

Figure 11. (A) XRD patterns of aged Pd/La(x)/Al_2O_3 (x = 0, 5, 15, 30 wt%). (B) S_{BET} of fresh and aged Pd/La(x)/Al_2O_3(x = 0, 5, 15, 30 wt%). S_{BET} for fresh Pd/Al_2O_3 and Pd/La(5)/Al_2O_3 were taken from our previous report.[27]

La K-edge XAFS measurements were carried out to further examine the local structure of La after hydrothermal aging (**Figure S9**). The results of a curve-fitting analysis of the EXAFS are summarized in **Table S4**. Pd/La(5)/Al_2O_3 revealed only two peaks at ca. 1.2 and 2.0 Å, even after aging. Again, the peak at 2.0 Å is due to the La–O bonds, while the other smaller peak is a side lobe of La–O due to the nonlinearity of their phase shifts.[44] A curve-fitting analysis showed that Pd/La(5)/Al_2O_3 contains only a La–O contribution after hydrothermal aging at 1000 °C. In contrast, La–Al and La–(O)–La contributions, which appear at ca. 2.9 and 3.5 Å in the EXAFS Fourier transforms, respectively, were observed for Pd/La(15)/Al_2O_3 and Pd/La(30)/Al_2O_3 after hydrothermal aging. Curve-fittings with both La–O and La–Al afforded better fits. These results indicate the formation of $LaAlO_3$ for Pd/La(15)/Al_2O_3 and Pd/La(30)/Al_2O_3 after hydrothermal aging at 1000 °C for 4 h. This result is in agreement with those of the aforementioned XRD measurements.

Figure S10 compares the conversion of NO, CO, and C_3H_6 at 300 °C of the studied honeycomb catalysts in the range λ = 1.05-0.95. The conversions were recorded after keeping each lambda condition for 1 min in order to examine the steady-state catalytic activity under these conditions. The conversion of NO occurred efficiently in the rich region ($0.95 \leq \lambda < 1$), where excess reducing gasses are present. We observed that Pd/La(15)/Al_2O_3 exhibited high NO-removal efficiency and its activity is comparable to Pd/La(5)/Al_2O_3 throughout the λ range tested in this investigation. On the other hand, the conversion of CO and C_3H_6 reached more than 80% in the lean region ($1 < \lambda \leq 1.05$), where

oxidation processes are preferred in the presence of excess O_2. Pd/La(15)/Al_2O_3 and Pd/La(5)/Al_2O_3 showed higher activity than Pd/La(30)/Al_2O_3 and Pd/Al_2O_3, which is consistent with the aforementioned investigations and demonstrates that i) La promotes the TWC process and that ii) an overload of La has a negative effect. It should also be noted here that Pd/La(5)/Al_2O_3 exhibited a slightly higher catalytic activity than Pd/La(15)/Al_2O_3 for the conversion of CO and C_3H_6.

Under realistic TWC conditions, the λ value fluctuates between low (rich) and high (lean) values.[61] It is thus highly important that the TWC catalysts can operate and efficiently remove the exhaust gases under such transient conditions and are able to follow the rapid changes of the λ conditions. Therefore, we investigated the λ-switching performance for NO, CO, and C_3H_6 on the honeycomb model catalysts (**Figure 12**). We started the investigation under lean conditions (λ = 1.05), before we switched to rich conditions, and finally changed again to lean conditions. It should be noted here that there are detection delays, which are due to the experimental setup (1.0 s for NO and 3.2 s for CO relative to C_3H_6). During the first change from lean to rich, the NO conversion over Pd/Al_2O_3 occurred faster than over the other catalysts, including Pd/La(15)/Al_2O_3. In contrast, for the subsequent change from rich to lean, a high NO conversion was retained the longest over Pd/La(15)/Al_2O_3. In addition, the NO conversion over Pd/Al_2O_3 gradually decreased under rich conditions, suggesting that CO acts as a poison for Pd as observed for the NO–CO reaction. These results indicate that the promotional effect of La i) is particularly effective under rich conditions, and ii) can be ineffective under lean conditions as Pd on La(15)/Al_2O_3 is more difficult to reduce than Pd on Al_2O_3 without La.

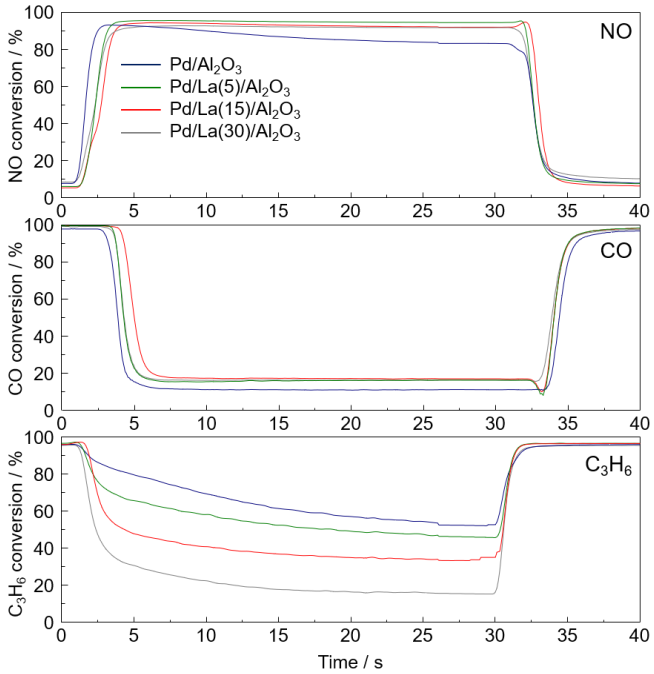

Figure 12. Lambda-switching performance for NO, CO, and C_3H_6 on the honeycomb model catalysts formed by coated Pd and alumina support materials upon lambda jumps (λ = 1.05-0.95). The time variation of the conversion rate was recorded with a data collection rate of 10 Hz. It should be noted here that there are detection delays due to the experimental setup (1.0 s for NO and 3.2 s for CO relative to C_3H_6).

Finally, practical tests using a commercial vehicle were carried out in order to confirm the applicability and potentially superior performance of Pd/La(15)/Al_2O_3 relative to the conventionally used catalyst Pd/La(5)/Al_2O_3. For this purpose, Pd-Rh three-way catalysts with a double-layered structure containing either Pd/La(15)/Al_2O_3 or Pd/La(5)/Al_2O_3 were prepared and bench aged for 75 h using a 1.8-L gasoline engine with a peak temperature of 950 °C. Subsequently, the catalysts were mounted in a commercial vehicle with a 1.5-L engine and evaluated according to the vehicle emission test of the LA-4 driving cycle. **Figure 13** shows the accumulated and transient emissions of NO_x, CO, and the total HC monitored at the tailpipe, as well as the AFR, and the catalyst-bed temperature together with the associated vehicle speed. **Figure 14** shows the corresponding transient emissions during the selected period (700-1000 s) for clarity. We observed that NO_x is mainly emitted during the acceleration of the vehicle for both practical tests. On the other hand, CO and HC are emitted during the deceleration of the vehicle, i.e., under AFR-rich conditions (AFR < 14.6) just after an excessive intake of air (fuel cut). Compared to the driving test using the conventional catalyst (Pd/La(5)/Al_2O_3; green line), the catalytic system including Pd/La(15)/Al_2O_3 (red line) shows improved conversions for all exhaust gasses. In particular, the conversion of NO_x was significantly improved by the incorporation of the increased amount of La.

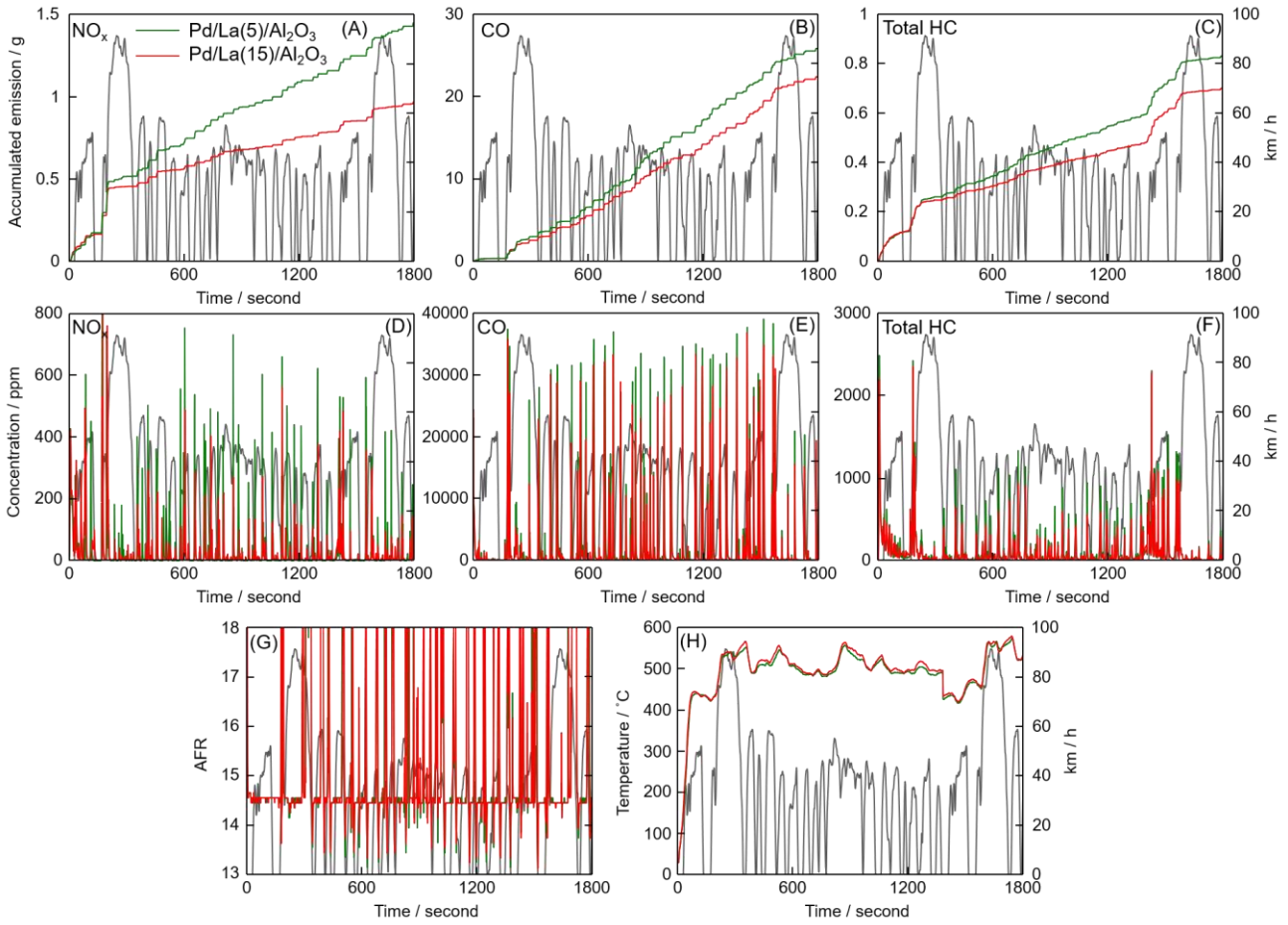

Figure 13. Accumulated emission of (A) NO_x, (B) CO, and (C) the total HC, monitored at the tailpipe during a LA-4 driving cycle (city cycle of US Federal and California) with a vehicle containing a 1.5-L

gasoline engine and a Pd-Rh three-way catalysts with Pd/La(5)/Al_2O_3 (green) or Pd/La(15)/Al_2O_3 (red). Corresponding transient emission of (D) NO_x, (E) CO, and (F) the total HC. (G) AFR, and (H) catalyst bed temperature.

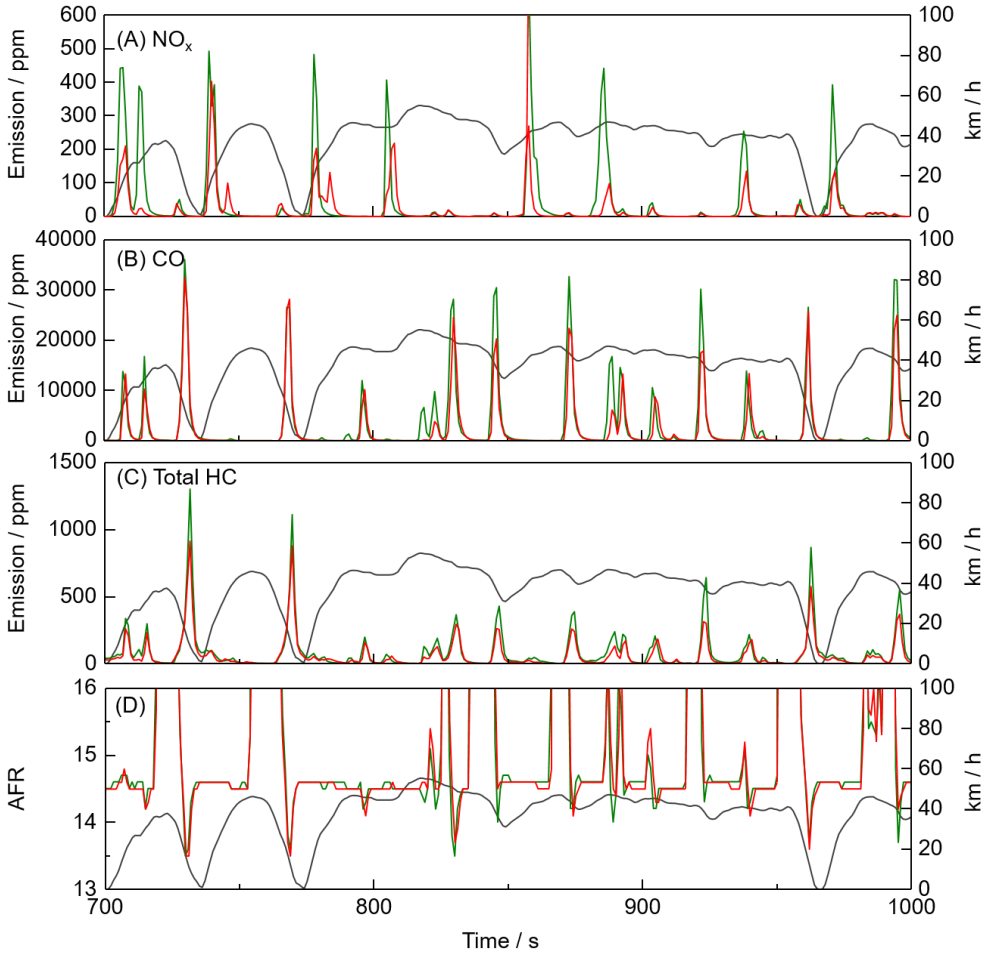

Figure 14. Transient emission of (A) NO_x, (B) CO, and (C) the total HC together with (D) AFR, monitored at the tailpipe during a LA-4 driving cycle (city cycle of US Federal and California) using a vehicle with a 1.5-L gasoline engine and a Pd-Rh three-way catalyst containing Pd/La(5)/Al_2O_3 (green) or Pd/La(15)/Al_2O_3 (red).

Conclusions

We have investigated the promotional effect of La in Pd/La(x)/Al_2O_3 (x = 0, 5, 15, 30wt%) catalysts for TWC reactions using a combination of kinetic and spectroscopic measurements as well as theoretical calculations. The obtained results show that the supported metallic Pd particles on La-containing Al_2O_3 supports are more electron deficient than those on pristine Al_2O_3, which results in a higher reactivity toward NO and a suppression of the poisoning effect of CO. As a result, a higher NO conversion efficiency is attained over these Pd/La/Al_2O_3 catalysts. In addition to investigations using powdered catalyst samples, we prepared and examined monolithic honeycomb catalyst samples in TWC reactions, which revealed a superior DeNO_x performance for Pd/La/Al_2O_3 compared to Pd/Al_2O_3. Moreover, we investigated the optimal La loading for TWC reactions and found that a loading of 15 wt%, which is higher than that for the conventionally used industrial catalysts Pd/La(5)/Al_2O_3 (La = 5wt%) optimized to keep the high specific surface area, is more effective for the TWC process. As this study is a collaborative academic and industrial effort, we have also performed a practical test using a commercial vehicle. The results show that the catalytic system containing Pd/La(15)/Al_2O_3 exhibits improved conversions for the exhaust gasses including NO_x, CO, and HC compared to the one containing Pd/La(5)/Al_2O_3. Our results thus indicate that the loading of La in Pd/La/Al_2O_3 catalysts should be tuned depending on the application systems. This tuning should consider a balance between the support stability in terms of the surface area and the promotional effect in the TWC process.

AUTHOR INFORMATION

Corresponding authors:

Takashi Toyao, Shuhei Nagaoka

E-mail: toyao@cat.hokudai.ac.jp; Shuhei.Nagaoka@mattheyasia.com

ASSOCIATED CONTENT

Supporting Information

The Supporting Information is available free of charge on the ACS Publications website at http://pubs.acs.org.

Composition of the simulated exhaust gas mixtures for TWC tests, additional experimental data, DFT calculations.

ACKNOWLEDGEMENTS

This study was financially supported by KAKENHI grants 17H01341, 18K14051, and 18K14057 from JSPS and by MEXT within the projects "IRCCS" and "ESICB", as well as by the JST CREST project JPMJCR17J3. The authors thank the technical division of the Institute for Catalysis (Hokkaido Univ.) for manufacturing experimental equipment. XAFS measurements were conducted at the BL-01B1 and BL-14B2 beamline facilities of SPring-8 at JASRI (proposal numbers 2018A1757 and 2018B1768). NAP-XPS experiments were carried out under the approval of the Photon Factory Program Advisory Committee (PF PAC No. 2015S2-008). Parts of the calculations were carried out on supercomputers at RIIT (Kyushu Univ.) and ACCMS (Kyoto Univ.).

References

(1) Wang, J.; Chen, H.; Hu, Z.; Yao, M.; Li, Y. A Review on the Pd-Based Three-Way Catalyst. *Catal. Rev.* **2015**, *57*, 79–144.

(2) Matsumoto, S. Recent Advances in Automobile Exhaust Catalysts. *Catal. Today* **2004**, *90*, 183–190.

(3) Shelef, M.; McCabe, R. W. Twenty-Five Years after Introduction of Automotive Catalysts: What Next? *Catal. Today* **2000**, *62*, 35–50.

(4) Yamamoto, T.; Tanaka, T.; Kuma, R.; Suzuki, S.; Amano, F.; Shimooka, Y.; Kohno, Y.; Funabiki, T.; Yoshida, S. NO Reduction with CO in the Presence of O_2 over Al_2O_3-Supported and Cu-Based Catalysts. *Phys. Chem. Chem. Phys.* **2002**, *4*, 2449–2458.

(5) Yoshida, H.; Yamashita, N.; Ijichi, S.; Okabe, Y.; Misumi, S.; Hinokuma, S.; Machida, M. A Thermally Stable Cr-Cu Nanostructure Embedded in the CeO_2 Surface as a Substitute for Platinum-Group Metal Catalysts. *ACS Catal.* **2015**, *5*, 6738−6747.

(6) Satsuma, A.; Ueda, K.; Ito, Y.; Ang, C. A.; Ohyama, J. Automotive Three Way Catalytic Activity of Fe–Ni/Ceria. *Chem. Lett.* **2015**, *44*, 703–705.

(7) Ueda, K.; Ohyama, J.; Satsuma, A. Investigation of Reaction Mechanism of NO-C_3H_6-CO-O_2 Reaction over $NiFe_2O_4$ Catalyst. *ACS Omega* **2017**, *2*, 3135−3143.

(8) Koga, H.; Tada, K.; Hayashi, A.; Ato, Y.; Okumura, M. High NO_x Reduction Activity of an Ultrathin Zirconia Film Covering a Cu Surface: A DFT Study. *Catal. Letters* **2017**, *147*, 1827–1833.

(9) Hosokawa, S.; Matsuki, K.; Tamaru, K.; Oshino, Y.; Aritani, H.; Asakura, H.; Teramura, K.; Tanaka, T. Selective Reduction of NO over Cu/Al_2O_3: Enhanced Catalytic Activity by Infinitesimal Loading of Rh on Cu/Al_2O_3. *Mol. Catal.* **2017**, *442*, 74–82.

(10) Iwachido, K.; Onodera, T.; Miyamoto, K. NO_x Trap Catalyst Technologies and Exhaust Emission Control to Expand Lean Burn Operation for Gasoline Engine Application. *Rev. Automot. Eng.* **2010**, 127–132.

(11) Machida, M.; Ueno, M.; Omura, T.; Kurusu, S.; Hinokuma, S.; Nanba, T.; Shinozaki, O.; Furutani, H. CeO_2-Grafted Mn-Fe Oxide Composites as Alternative Oxygen-Storage Materials for Three-Way Catalysts: Laboratory and Chassis Dynamometer Tests. *Ind. Eng. Chem. Res.* **2017**, *56*, 3184−3193.

(12) Suarez-Bertoa, R.; Astorga, C. Impact of Cold Temperature on Euro 6 Passenger Car Emissions. *Environ. Pollut.* **2018**, *234*, 318–329.

(13) Li, L.; Zhang, N.; Huang, X.; Liu, Y.; Li, Y.; Zhang, G.; Song, L.; He, H. Hydrothermal Stability of Core-Shell $Pd@Ce_{0.5}Zr_{0.5}O_2/Al_2O_3$ Catalyst for Automobile Three-Way Reaction. *ACS Catal.* **2018**, *8*, 3222−3231.

(14) Gandhi, H. S.; Graham, G. W.; McCabe, R. W. Automotive Exhaust Catalysis. *J. Catal.* **2003**, *216*, 433–442.

(15) Kang, S. B.; Nam, I. S.; Cho, B. K.; Kim, C. H.; Oh, S. H. Kinetic Model for Modern Double-Layered Pd/Rh TWC as a Function of Metal Loadings and Mileage. *Chem. Eng. J.* **2015**, *278*, 328–338.

(16) Nishio, Y.; Ozawa, M. Thermal Stability and Microstructural Change of Lanthanum Modified Alumina Catalytic Support. *J. Ceram. Soc. Japan* **2007**, *115*, 633–636.

(17) Muraki, H.; Shinjoh, H.; Fujitani, Y. Effect of Lanthanum on the No Reduction over Palladium Catalysts. *Appl. Catal.* **1986**, *22*, 325–335.

(18) Muraki, H.; Shinjoh, H.; Sobukawa, H.; Yokota, K.; Fujitani, Y. Palladium-Lanthanum Catalysts for Automotive Emission Control. *Ind. Eng. Chem. Prod. Res. Dev.* **1986**, *25*, 202–208.

(19) Muraki, H.; Yokota, K.; Fujitani, Y. Nitric Oxide Reduction Performance of Automotive Palladium Catalysts. *Appl. Catal.* **1989**, *48*, 93–105.

(20) Shinjoh, H. Rare Earth Metals for Automotive Exhaust Catalysts. *J. Alloys Compd.* **2006**, *408–412*, 1061–1064.

(21) Shinjoh, H.; Isomura, N.; Sobukawa, H.; Sugiura, M. Effect of Alkaline Addition on Hydrocarbon Oxidation Activities of Palladium Three-Way Catalyst. *Stud. Surf. Sci. Catal.* **1998**, *116*, 83–91.

(22) Kobayashi, T.; Yamada, T.; Kayano, K. Effect of Basic Metal Additives on NO x Reduction Property of Pd-Based Three-Way Catalyst. *Appl. Catal. B Environ.* **2001**, *30*, 287–292.
(23) Graham, G. W. NO Chemisorption on Supported Pd. *Surf. Sci.* **1992**, *268*, 25–35.
(24) David Logan, A.; Graham, G. W. NO Chemisorption on Pd(100) with Ultra-Thin Overlayers of Oxidized La and Al. *Surf. Sci. Lett.* **1992**, *277*, L47–L51.
(25) Sekiba, T.; Kimura, S.; Yamamoto, H.; Okada, A. Development of Automotive Palladium Three-Way Catalysts. *Catal. Today* **1994**, *22*, 113–126.
(26) Skoglundh, M.; Johansson, H.; Löwendahl, L.; Jansson, K.; Dahl, L.; Hirschauer, B. Cobalt-Promoted Palladium as a Three-Way Catalyst. *Appl. Catal. B Environ.* **1996**, *7*, 299–319.
(27) Toyao, T.; Jing, Y.; Kon, K.; Hayama, T.; Nagaoka, S.; Shimizu, K. Catalytic NO–CO Reactions over La-Al_2O_3 Supported Pd: Promotion Effect of La. *Chem. Lett.* **2018**, *47*, 1036–1039.
(28) Valden, M.; Keiski, R. L.; Xiang, N.; Pere, J.; Aaltonen, J.; Pessa, M.; Maunula, T.; Savimäki, A.; Lahti, A.; Härkönen, M. Reactivity of Pd/Al_2O_3, Pd/La_2O_3-Al_2O_3 and Pd/$LaAlO_3$ Catalysts for the Reduction of NO by CO: CO and NO Adsorption. *J. Catal.* **1996**, *161*, 614–625.
(29) Takagi, N.; Ishimura, K.; Miura, H.; Shishido, T.; Fukuda, R.; Ehara, M.; Sakaki, S. Catalysis of Cu Cluster for NO Reduction by CO: Theoretical Insight into the Reaction Mechanism. *ACS Omega* **2019**, *4*, 2596–2609.
(30) Toyoshima, A.; Kikuchi, T.; Tanaka, H.; Mase, K.; Amemiya, K.; Ozawa, K. Performance of PF BL-13A, a Vacuum Ultraviolet and Soft X-Ray Undulator Beamline for Studying Organic Thin Films Adsorbed on Surfaces. *J. Phys. Conf. Ser.* **2013**, *425*, 152019−152022.
(31) Aderhold, D.; Haynes, A. G.; Spencer, M. L. W.; Winterborn, D. J. W. Monolith Coating Apparatus and Method Therefor. *US Pat.* **2013**, *US6599570B*.
(32) Kresse, G.; Furthmüller, J. Efficient Iterative Schemes for Ab Initio Total-Energy Calculations Using a Plane-Wave Basis Set. *Phys. Rev. B - Condens. Matter Mater. Phys.* **1996**, *54*, 11169–11186.
(33) Kresse, G.; Furthmüller, J. Efficiency of Ab-Initio Total Energy Calculations for Metals and Semiconductors Using a Plane-Wave Basis Set. *Comput. Mater. Sci.* **1996**, *6*, 15–50.
(34) Blöchl, P. E. Projector Augmented-Wave Method. *Phys. Rev. B* **1994**, *50*, 17953–17979.
(35) Perdew, J. P.; Burke, K.; Ernzerhof, M. Generalized Gradient Approximation Made Simple. *Phys. Rev. Lett.* **1996**, *77*, 3865–3868.
(36) Grimme, S.; Antony, J.; Ehrlich, S.; Krieg, H. A Consistent and Accurate Ab Initio Parametrization of Density Functional Dispersion Correction (DFT-D) for the 94 Elements H-Pu. *J. Chem. Phys.* **2010**, *132*, 154104.
(37) Grimme, S.; Ehrlich, S.; Goerigk, L. Effect of the Damping Function in Dispersion Corrected Density Functional Theory. *J. Comput. Chem.* **2011**, *32*, 1456–1465.
(38) Hu, C. H.; Chizallet, C.; Mager-Maury, C.; Corral-Valero, M.; Sautet, P.; Toulhoat, H.; Raybaud, P. Modulation of Catalyst Particle Structure upon Support Hydroxylation: Ab Initio Insights into Pd_{13} and Pt_{13}/γ-Al_2O_3. *J. Catal.* **2010**, *274*, 99–110.
(39) Kwak, J. H.; Hu, J.; Lukaski, A.; Kim, D. H.; Szanyi, J.; Peden, C. H. F. Role of Pentacoordinated Al^{3+} Ions in the High Temperature Phase Transformation of γ-Al_2O_3. *J. Phys. Chem. C* **2008**, *112*, 9486–9492.
(40) Düvel, A.; Romanova, E.; Sharifi, M.; Freude, D.; Wark, M.; Heitjans, P.; Wilkening, M. Mechanically Induced Phase Transformation of γ-Al_2O_3 into α-Al_2O_3. Access to Structurally Disordered γ-Al_2O_3 with a Controllable Amount of Pentacoordinated Al Sites. *J. Phys. Chem. C* **2011**, *115*, 22770–22780.
(41) Wischert, R.; Florian, P.; Copéret, C.; Massiot, D.; Sautet, P. Visibility of Al Surface Sites of γ-Alumina: A Combined Computational and Experimental Point of View. *J. Phys. Chem. C* **2014**, *118*, 15292−15299.
(42) Boukha, Z.; Fitian, L.; López-Haro, M.; Mora, M.; Ruiz, J. R.; Jiménez-Sanchidrián, C.; Blanco, G.; Calvino, J. J.; Cifredo, G. A.; Trasobares, S.; Bernal, S. Influence of the Calcination Temperature on the Nano-Structural Properties, Surface Basicity, and Catalytic Behavior of Alumina-Supported Lanthana Samples. *J. Catal.* **2010**, *272*, 121–130.
(43) Ferrandon, M.; Björnbom, E. Hydrothermal Stabilization by Lanthanum of Mixed Metal Oxides and Noble Metal Catalysts for Volatile Organic Compound Removal. *J. Catal.* **2001**, *200*,

148–159.
(44) Yamamoto, T.; Hatsui, T.; Matsuyama, T.; Tanaka, T.; Funabiki, T. Structures and Acid-Base Properties of La/Al_2O_3- Role of La Addition to Enhance Thermal Stability of γ-Al_2O_3. *Chem. Mater.* **2003**, *15*, 4830–4840.
(45) Wang, S.; Borisevich, A. Y.; Rashkeev, S. N.; Glazoff, M. V.; Sohlberg, K.; Pennycook, S. J.; Pantelides, S. T. Dopants Adsorbed as Single Atoms Prevent Degradation of Catalysts. *Nat. Mater.* **2004**, *3*, 143–146.
(46) Peterson, E. J.; DeLaRiva, A. T.; Lin, S.; Johnson, R. S.; Guo, H.; Miller, J. T.; Kwak, J. H.; Peden, C. H. F.; Kiefer, B.; Allard, L. F.; Ribeiro, F. H.; Datye, A. K. Low-Temperature Carbon Monoxide Oxidation Catalysed by Regenerable Atomically Dispersed Palladium on Alumina. *Nat. Commun.* **2014**, *5*, 4885.
(47) Wang, H.; Dong, J.; Allard, L. F.; Lee, S.; Oh, S.; Wang, J.; Li, W.; Shen, M.; Yang, M. Single-Site Pt/La-Al_2O_3 Stabilized by Barium as an Active and Stable Catalyst in Purifying CO and C_3H_6 Emissions. *Appl. Catal. B Environ.* **2019**, *244*, 327–339.
(48) Berlowitz, P. J.; Peden, C. H. F.; Goodman, D. W. Kinetics of CO Oxidation on Single-Crystal Pd, Pt, and Ir. *J. Phys. Chem.* **1988**, *92*, 5213–5221.
(49) Gajdoš, M.; Eichler, A.; Hafner, J. CO Adsorption on Close-Packed Transition and Noble Metal Surfaces: Trends from Ab Initio Calculations. *J. Phys. Condens. Matter* **2004**, *16*, 1141–1164.
(50) Zeinalipour-Yazdi, C. D.; Cooksy, A. L.; Efstathiou, A. M. CO Adsorption on Transition Metal Clusters: Trends from Density Functional Theory. *Surf. Sci.* **2008**, *602*, 1858–1862.
(51) Asakura, H.; Hosokawa, S.; Ina, T.; Kato, K.; Nitta, K.; Uera, K.; Uruga, T.; Miura, H.; Shishido, T.; Ohyama, J.; Satsuma, A.; Sato, K.; Yamamoto, A.; Hinokuma, S.; Yoshida, H.; Machida, M.; Yamazoe, S.; Tsukuda, T.; Teramura, K.; Tanaka, T. Dynamic Behavior of Rh Species in Rh/Al_2O_3 Model Catalyst during Three-Way Catalytic Reaction: An Operando X-Ray Absorption Spectroscopy Study. *J. Am. Chem. Soc.* **2018**, *140*, 176–184.
(52) Goodman, E. D.; Johnston-Peck, A. C.; Dietze, E. M.; Wrasman, C. J.; Hoffman, A. S.; Abild-Pedersen, F.; Bare, S. R.; Plessow, P. N.; Cargnello, M. Catalyst Deactivation via Decomposition into Single Atoms and the Role of Metal Loading. *Nat. Catal.* **2019**, *2*, 748–755.
(53) Pieta, I. S.; García-Diéguez, M.; Herrera, C.; Larrubia, M. A.; Alemany, L. J. In Situ DRIFT-TRM Study of Simultaneous NOx and Soot Removal over Pt-Ba and Pt-K NSR Catalysts. *J. Catal.* **2010**, *270*, 256–267.
(54) Chi, Y.; Chuang, S. S. C. Infrared and TPD Studies of Nitrates Adsorbed on Tb_4O_7, La_2O_3, BaO, and MgO/γ-Al_2O_3. *J. Phys. Chem. B* **2000**, *104*, 4673–4683.
(55) Lietti, L.; Daturi, M.; Blasin-Aubé, V.; Ghiotti, G.; Prinetto, F.; Forzatti, P. Relevance of the Nitrite Route in the NO_x Adsorption Mechanism over Pt-Ba/Al_2O_3 NO_x Storage Reduction Catalysts Investigated by Using Operando FTIR Spectroscopy. *ChemCatChem* **2012**, *4*, 55–58.
(56) Haneda, M.; Kintaichi, Y.; Nakamura, I.; Fujitani, T.; Hamada, H. Effect of Surface Structure of Supported Palladium Catalysts on the Activity for Direct Decomposition of Nitrogen Monoxide. *J. Catal.* **2003**, *218*, 405–410.
(57) Polzonetti, G.; Alnot, P.; Brundle, C. R. The Adsorption and Reactions of NO_2 on the Ag(111) Surface. I. XPS/UPS and Annealing Studies between 90 and 300 K. *Surf. Sci.* **1990**, *238*, 226–236.
(58) Ueda, K.; Isegawa, K.; Amemiya, K.; Mase, K.; Kondoh, H. Operando NAP-XPS Observation and Kinetics Analysis of NO Reduction over Rh(111) Surface: Characterization of Active Surface and Reactive Species. *ACS Catal.* **2018**, *8*, 11663−11670.
(59) Kim, D.; Woo, S.; Lee, J.; Yang, O. The Role of Lanthanum Oxide on Pd - only Three - way Catalysts Prepared by Co - impregnation and Sequential Impregnation Methods. *Catal. Letters* **2000**, *70*, 35–41.
(60) Takayama, A.; Kurokawa, T.; Nakayama, H.; Katoh, T.; Nagata, M. Effect of Ba and La Additives to the Pd Layer of a Pd:Rh TWC. *SAE Tech. Pap.* **2017**, 2017-01–0922.
(61) Farrauto, R. J.; Heck, R. M. Catalytic Converters: State of the Art and Perspectives. *Catal.*

Today **1999**, *51*, 351–360.

TOC

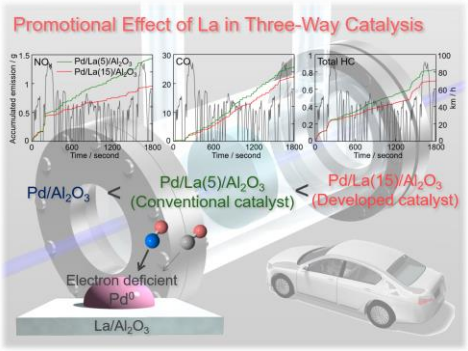

(6.26 cm × 4.75 cm)